

Paper

Augmented phase reduction for periodic orbits near a homoclinic bifurcation and for relaxation oscillators

Bharat Monga^{1a)} and Jeff Moehlis¹

¹ *Department of Mechanical Engineering, Engineering II Building, University of California Santa Barbara, Santa Barbara, CA 93106 USA*

^{a)} *monga@ucsb.edu*

Received May 24, 2020; Revised September 25, 2020; Published January 1, 2021

Abstract: Oscillators - dynamical systems with stable periodic orbits - arise in many systems of physical, technological, and biological interest. The standard phase reduction, a model reduction technique based on isochrons, can be unsuitable for oscillators which have a small-magnitude negative nontrivial Floquet exponent. This necessitates the use of the augmented phase reduction, a recently devised two-dimensional reduction technique based on isochrons and isostables. In this article, we calculate analytical expressions for the augmented phase reduction for two dynamically different planar systems: periodic orbits born out of homoclinic bifurcation, and relaxation oscillators. To validate our calculations, we simulate models in these dynamic regimes, and compare their numerically computed augmented phase reduction with the derived analytical expressions. These analytical and numerical calculations help us to understand conditions for which the use of augmented phase reduction over the standard phase reduction can be advantageous.

Key Words: isostables, isochrons, bifurcation theory, isostable response curve, phase response curve

1. Introduction

Periodic orbits are fundamentally important in dynamical systems theory, and they are intimately tied to other fundamental concepts such as bifurcations and chaos. Beyond their theoretical interest, they arise in many crucial physical, biological, and technological applications, from mechanical oscillations to electrical circuits to circadian rhythms to neural activity. Standard phase reduction [1–4], a classical reduction technique based on isochrons [2], has been instrumental in understanding such oscillatory systems. It reduces the dimensionality of a dynamical system with a periodic orbit to a single phase variable, and captures the oscillator’s phase change due to an external perturbation through the phase response curve (PRC). This can make the analysis of high dimensional systems more tractable, and their control [5–10] experimentally implementable; see e.g., [7, 11–13]. This is because although the whole state space dynamics of the system may not be known, the PRC can often be measured experimentally; see e.g., [9, 14].

Standard phase reduction is valid only in a small neighborhood of the periodic orbit. Consequently, the magnitude of the allowable perturbation is limited by the nontrivial Floquet exponents [15] of the periodic orbit: in systems with a small-magnitude negative nontrivial Floquet exponent, even a relatively small perturbation can lead to a trajectory which stays away from the periodic orbit, rendering the phase reduction inaccurate and phase reduction based control ineffective. This necessitates the use of a new reduction technique called augmented phase reduction [16], a two-dimensional reduction based on both isochrons and isostables [17]. While the first dimension captures the phase of the oscillator along the periodic orbit, like the standard phase reduction, the second dimension captures the oscillator’s transversal approach to the periodic orbit. This reduction ascertains the effect of an external stimulus on the oscillator’s phase change through the PRC, and the change in its transversal distance to the periodic orbit through the isostable response curve (IRC). A similar reduction was derived in [18] using Koopman operator techniques. We follow the reduction derived in [16] for our analysis in this article. Control algorithms based on the augmented phase reduction are expected to be more effective [16, 19], as they can be designed to allow a larger stimulus without the risk of driving the oscillator too far away from the periodic orbit. We envision that IRCs can be measured experimentally just like PRCs, making the control based on the augmented phase reduction experimentally amenable as well.

To understand dynamic regimes for which it could be advantageous to use the augmented phase reduction over the standard phase reduction, it is useful to analyze phase reduction for distinct dynamical systems that give rise to a periodic orbit. To simplify our analysis, we restrict to planar dynamical systems, and note that our analysis could be extended to higher dimensional systems with appropriate modifications. In [10], we derived analytical expressions for the augmented phase reduction for four such dynamical systems: $\lambda - \omega$ systems, the normal form for a supercritical Hopf bifurcation, the normal form of a Bautin bifurcation which has a saddle-node bifurcation of limit cycles, and simple two-dimensional models undergoing SNIPER bifurcations. Our contribution there was the analytical calculation of IRCs and the nontrivial Floquet exponent for each of these systems, and the PRC for a simple model undergoing a SNIPER bifurcation. That study showed that $\lambda - \omega$, Hopf, and Bautin normal form systems have sinusoidal PRCs and IRCs. Moreover, for the model near a SNIPER bifurcation, the PRC never changes sign, while the IRC looks like a skewed sinusoid. From such calculations, we concluded that it is advantageous to use augmented phase reduction over the standard phase reduction for systems having dynamics similar to these dynamical systems.

In this paper we consider two additional dynamical systems, distinct from the aforementioned dynamical systems analyzed in [10]: systems in which periodic orbits are born out of homoclinic bifurcations, and relaxation oscillators. The first of these represents another way in which a stable periodic orbit can arise from a codimension one bifurcation [15, 20], and the second is a common type of oscillation for systems of biological interest [21]. Our contribution in this paper is the analytical calculation of IRCs and the nontrivial Floquet exponent for each of these two systems. Our approach for the IRC calculation for a relaxation oscillator is in line with Izhikevich’s analysis [22] for the calculation of the PRC for such systems. To validate our calculations, we simulate examples of such systems, and compare their numerically computed augmented phase reduction with the derived analytical expressions. These results together with the results in [10] give a useful catalog of analytical results for the augmented phase reduction for planar dynamical systems having a stable periodic orbit.

This article is organized as follows. In Section 2, we introduce standard and augmented phase reduction. In Section 3, we analytically calculate the augmented phase reduction for the two systems, and simulate two different models under the appropriate regimes to validate our calculations. Section 4 concludes the article by summarizing the derived analytical expressions and discussing their implications.

2. Standard and augmented phase reduction

In this section, we give background on the concepts of isochrons, isostables, and standard and augmented phase reduction. These concepts will be used to calculate the IRC expressions in Section 3.

2.1 Standard phase reduction

The standard phase reduction is a classical technique used to describe dynamics near a periodic orbit by reducing the dimensionality of a dynamical system to a single phase variable θ [1, 3]. Consider a general n -dimensional dynamical system given by

$$\frac{d\mathbf{x}}{dt} = F(\mathbf{x}), \quad \mathbf{x} \in \mathbb{R}^n, \quad (n \geq 2). \quad (1)$$

Suppose this system has a stable periodic orbit $\gamma(t)$ with period T . For each point \mathbf{x}^* in the basin of attraction of the periodic orbit, there exists a corresponding phase $\theta(\mathbf{x}^*)$ such that [1–4, 10]

$$\lim_{t \rightarrow \infty} \left| \mathbf{x}(t) - \gamma \left(t + \frac{T}{2\pi} \theta(\mathbf{x}^*) \right) \right| = 0, \quad (2)$$

where $\mathbf{x}(t)$ is the flow of the initial point \mathbf{x}^* under the given vector field. The function $\theta(\mathbf{x})$ is called the *asymptotic phase* of \mathbf{x} , and takes values in $[0, 2\pi)$. *Isochrons* are level sets of this phase function. It is typical to define isochrons so that the phase of a trajectory advances linearly in time. This implies

$$\frac{d\theta}{dt} = \frac{2\pi}{T} \equiv \omega \quad (3)$$

both on and off the periodic orbit. Now consider the system

$$\frac{d\mathbf{x}}{dt} = F(\mathbf{x}) + U(t), \quad \mathbf{x} \in \mathbb{R}^n, \quad (4)$$

where $U(t) \in \mathbb{R}^n$ is an external perturbation. Standard phase reduction can be used to reduce this system to a one dimensional system given by [4]:

$$\dot{\theta} = \omega + \mathcal{Z}(\theta)^T U(t). \quad (5)$$

Here $\mathcal{Z}(\theta) \equiv \nabla_{\gamma(t)} \theta \in \mathbb{R}^n$ is the gradient of phase variable θ evaluated on the periodic orbit and is referred to as the (*infinitesimal*) *phase response curve (PRC)*. It quantifies the effect of an external perturbation on the phase of a periodic orbit. The PRC can be found by solving an adjoint equation numerically [4, 23, 24]:

$$\frac{d\nabla_{\gamma(t)} \theta}{dt} = -DF^T(\gamma(t)) \nabla_{\gamma(t)} \theta, \quad (6)$$

subject to the initial condition

$$\nabla_{\gamma(0)} \theta \cdot F(\gamma(0)) = \omega. \quad (7)$$

Here DF is the Jacobian of F evaluated on the periodic orbit. Since $\nabla_{\gamma(t)} \theta$ evolves in \mathbb{R}^n , (7) supplies only one of n required initial conditions; the rest arise from requiring that the solution $\nabla_{\gamma(t)} \theta$ to (6) be T -periodic. This adjoint equation can be solved numerically with the program XPP [25] to find the PRC Q_{XPP} . Since XPP computes the PRC in terms of the change in time instead of the change in phase, we rescale the XPP PRC Q_{XPP} as

$$\nabla_{\gamma} \theta = \omega Q_{\text{XPP}}.$$

Equation (5) is valid only in a small neighborhood of the periodic orbit, and diverges from the true dynamics as one goes further away from the periodic orbit. Therefore, the amplitude of an external perturbation has to be small enough so that it does not drive the system far away from the periodic orbit where the phase reduction is not accurate. This limitation becomes even more important if the nontrivial Floquet exponent of the periodic orbit is a negative number small in magnitude [19]. This limits the achievement of certain control objectives and thus necessitates the use of the augmented phase reduction.

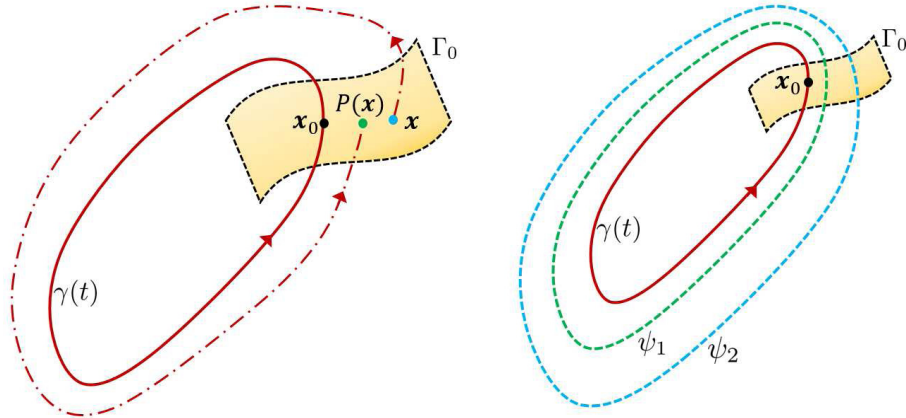


Fig. 1. Isostables for a periodic orbit. The left panel shows the Poincaré map P on the isochron Γ_0 of the periodic orbit $\gamma(t)$. The trajectory starting from \mathbf{x} on the isochron lands back on the isochron at $P(\mathbf{x})$ after one period. The right panel visualizes the isostables as giving a sense of transversal distance from the periodic orbit by showing two isostable level sets ψ_1 and ψ_2 .

2.2 Augmented phase reduction

For systems which have a stable fixed point, it can be useful to define *isostables* [17], which are sets of points in phase space that approach the fixed point together and are analogous to isochrons for asymptotically periodic systems. Isostables are related to the eigenfunctions of the Koopman operator [17]. Such a notion of isostables was recently adapted for systems having a stable periodic orbit [16], where isostables were defined to be the set of points that approach a periodic orbit together. They give a sense of the distance in directions transverse to the periodic orbit, visualized in the right panel of Fig. 1. Standard phase reduction can be augmented with these coordinates as follows.

Consider a point \mathbf{x}_0 on the periodic orbit $\gamma(t)$ with the corresponding isochron Γ_0 . The transient behavior of the system (1) near \mathbf{x}_0 can be analyzed by a Poincaré map P on Γ_0 ,

$$P : \Gamma_0 \rightarrow \Gamma_0; \quad \mathbf{x} \rightarrow P(\mathbf{x}). \quad (8)$$

This is shown in the left panel of Fig. 1. Here \mathbf{x}_0 is a fixed point of this map, and we can approximate P in a small neighborhood of \mathbf{x}_0 as

$$P(\mathbf{x}) = \mathbf{x}_0 + DP(\mathbf{x} - \mathbf{x}_0) + O(\|\mathbf{x} - \mathbf{x}_0\|^2), \quad (9)$$

where $DP = dP/dx|_{\mathbf{x}_0}$. Suppose DP is diagonalizable with $V \in \mathbb{R}^{n \times n}$ as a matrix with columns of unit length eigenvectors $\{v_i | i = 1, \dots, n\}$ and the associated real eigenvalues $\{\lambda_i | i = 1, \dots, n\}$ of DP . These eigenvalues λ_i are the Floquet multipliers of the periodic orbit. (Since we will focus our analysis on planar dynamical systems in this paper, our assumption that the Floquet multipliers are real will always hold. One could modify the analysis in line with [26] to account for complex Floquet multipliers in higher dimensional systems.) For every nontrivial Floquet multiplier λ_i , with the corresponding eigenvector v_i , the set of isostable coordinates is defined as [16]

$$\psi_i(\mathbf{x}) = e_i^T V^{-1}(\mathbf{x}_\Gamma - \mathbf{x}_0) \exp(-\log(\lambda_i)t_\Gamma/T), \quad (10)$$

where $i = 1, \dots, n-1$. Here \mathbf{x}_Γ and $t_\Gamma \in [0, T)$ are defined to be the position and the time at which the trajectory first returns to the isochron Γ_0 , and e_i is a vector with 1 in the i^{th} position and 0 elsewhere. As shown in [16], we get the following equations for ψ_i and its gradient $\nabla_{\gamma(t)}\psi_i$ under the flow $\dot{\mathbf{x}} = F(\mathbf{x})$:

$$\dot{\psi}_i = k_i \psi_i, \quad (11)$$

$$\frac{d\nabla_{\gamma(t)}\psi_i}{dt} = (k_i I - DF(\gamma(t))^T) \nabla_{\gamma(t)}\psi_i, \quad (12)$$

where $k_i = \log(\lambda_i)/T$ is the i^{th} nontrivial Floquet exponent, and I is the identity matrix. We refer to this gradient $\nabla_{\gamma(t)}\psi_i \equiv \mathcal{I}_i(\theta)$ as the *isostable response curve (IRC)*. Its T -periodicity along with

the normalization condition $\nabla_{\mathbf{x}_0} \psi_i \cdot v_i = 1$ gives a unique IRC. It gives a measure of the effect of a control input in driving the trajectory away from the periodic orbit. The n -dimensional system (given by (4)) can be realized as [16]

$$\dot{\theta} = \omega + \mathcal{Z}^T(\theta)U(t), \quad (13)$$

$$\dot{\psi}_i = k_i \psi_i + \mathcal{I}_i^T(\theta)U(t), \quad \text{for } i = 1, \dots, n-1. \quad (14)$$

We refer to this reduction as the augmented phase reduction; it is valid in the limit of small control inputs $U(t)$. Here, the phase variable θ indicates the position of the trajectory along the periodic orbit, and the isostable coordinate ψ_i gives information about transversal distance from the periodic orbit along the i^{th} eigenvector v_i . It is evident from (13, 14) that an external perturbation affects the oscillator's phase through the PRC, and its transversal distance to the periodic orbit through the IRC. In practice, isostable coordinates with nontrivial Floquet multiplier close to 0 can be ignored as perturbations in those directions are nullified quickly under the evolution of the vector field. If all isostable coordinates are ignored, the augmented phase reduction reduces to the standard phase reduction. In this paper, the models that we calculate the augmented phase reduction for are two-dimensional, so there is only one isostable coordinate. We thus write the adjoint equation as

$$\frac{d\nabla_{\gamma(t)}\psi}{dt} = (kI - DF(\gamma(t))^T) \nabla_{\gamma(t)}\psi, \quad (15)$$

and the augmented phase reduction as

$$\dot{\theta} = \omega + \mathcal{Z}^T(\theta)U(t), \quad (16)$$

$$\dot{\psi} = k\psi + \mathcal{I}^T(\theta)U(t). \quad (17)$$

We have removed the subscript for ψ , k , and \mathcal{I} as we only have one isostable coordinate. The eigenvector v is then the unit vector along the one-dimensional isochron Γ_0 . The nontrivial Floquet exponent k can then be computed from the divergence of the vector field as [27]

$$k = \frac{\int_0^T \nabla \cdot F(\gamma(t))dt}{T}. \quad (18)$$

We note that [28] shows how the augmented phase reduction can be extended to include higher order corrections.

3. Analytical and numerical computation of the augmented phase reduction

Bifurcation theory [15, 20] identifies four codimension one bifurcations which give birth to a stable limit cycle for generic families of vector fields: a supercritical Hopf bifurcation, a saddle-node bifurcation of limit cycles, a SNIPER bifurcation (saddle-node bifurcation of fixed points on a periodic orbit, also called a SNIC bifurcation), and a homoclinic bifurcation. Analytical calculations for the augmented phase reduction of systems undergoing the first three of these bifurcations are given in [10]. In this section, we derive analytical expressions for the augmented phase reduction of planar dynamical systems which have a stable limit cycle which arises from a homoclinic bifurcation, and also for systems with relaxation oscillators with fast-slow dynamics.

To validate our calculations, we simulate two different models whose dynamics are expected to be captured by the aforementioned planar systems, and we compare their numerically computed IRCs with the derived analytical expressions. In the numerical computation of the IRCs for the planar systems, we directly calculate the nontrivial Floquet exponent k as the mean of the divergence of vector field along the periodic orbit according to (18). On the other hand, for higher dimensional models, we first compute PRC using the software XPP [25], then choose an arbitrary point on the periodic orbit as $\theta = 0$, and approximate the isochron as a hyperplane orthogonal to the PRC at that point. To compute the Jacobian DP , we compute \mathbf{x}_Γ for a number of initial conditions \mathbf{x}_0 spread out

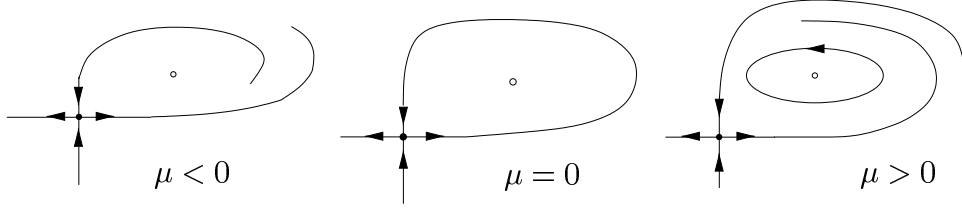


Fig. 2. A homoclinic orbit exists at $\mu = 0$, giving rise to a stable periodic orbit for $\mu > 0$.

on the isochron. Eigenvector decomposition of DP gives us the Floquet multipliers of the periodic orbit and thus k . After obtaining k , we use Newton iteration to obtain the IRC as the periodic solution to (15). Note that the PRC and the IRC for higher dimensional systems can also be computed in the context of the Koopman operator, by computing Fourier and Laplace averages evaluated along the system trajectories [29]. The higher dimensional systems we consider for numerical simulation in this section have only one negative small magnitude nontrivial Floquet exponent, so the reduction given by (16,17) still applies.

3.1 Homoclinic bifurcation

For a homoclinic bifurcation [15, 20], a periodic orbit is born out of a homoclinic orbit to a hyperbolic saddle point p upon varying a parameter μ . We will consider planar systems with a homoclinic bifurcation. If a homoclinic orbit exists for $\mu = 0$, then there will be a periodic orbit for, say, $\mu > 0$, but not for $\mu < 0$, as shown in Fig. 2. We assume that the magnitude of the unstable eigenvalue λ_u of the saddle point is smaller than the stable eigenvalue λ_s , resulting in a stable periodic orbit [15]. Moreover, we will assume that the periodic orbit is strongly attracting, that is, that $|\lambda_s/\lambda_u|$ is sufficiently large that a trajectory perturbed away from the periodic orbit will return to an infinitesimal neighborhood of the periodic orbit after one transit around the periodic orbit; see [30] for a discussion of a related piecewise continuous system which shows that there can be corrections to the phase response curve if the periodic orbit is not strongly attracting, and multiple transits need to be considered.

For μ close to zero, the periodic solution spends most of its time near the saddle point p , where the vector field can be approximated by its linearization. It can be written in diagonal form as

$$\dot{x} = \lambda_u x, \quad (19)$$

$$\dot{y} = \lambda_s y, \quad (20)$$

where $\lambda_u > 0$, and $\lambda_s < 0$. As in [4], we consider a box $B = [0, \Delta] \times [0, \Delta] \equiv \Sigma_0 \times \Sigma_1$ that encloses the periodic orbit for most of its time period, and within which (19, 20) are accurate. This is shown in the left panel of Fig. 3. We do not model the periodic orbit outside B , but assume that trajectory re-enters the box after a time δT at a distance ϵ from the y axis, where ϵ varies with the bifurcation parameter μ . The time taken for the trajectory to traverse B can be found as [4]

$$\tau(\epsilon) = \frac{1}{\lambda_u} \log \left(\frac{\Delta}{\epsilon} \right). \quad (21)$$

Thus the time period T of the periodic orbit is given as $\tau(\epsilon) + \delta T$. As μ decreases towards zero, the periodic orbit approaches p , resulting in ϵ approaching 0. Near the bifurcation, $\delta T \ll \tau(\epsilon)$, so $T \approx \tau(\epsilon)$. We approximate the trajectory as spending all its time within the box B , and re-injecting into the box instantaneously. Thus we set $\theta = 0$ at the point where trajectory enters B , and $\theta = 2\pi$ where trajectory exits B . To find the PRC, we solve the adjoint equation in B to get

$$\mathcal{Z}(\theta) = \mathcal{Z}_{x_0} e^{-\lambda_u t} \hat{x} + \mathcal{Z}_{y_0} e^{-\lambda_s t} \hat{y}, \quad (22)$$

subject to the initial condition (Eq. (7))

$$\mathcal{Z}_{x_0} \lambda_u \epsilon + \mathcal{Z}_{y_0} \lambda_s \Delta = \frac{2\pi \lambda_u}{\log \left(\frac{\Delta}{\epsilon} \right)}. \quad (23)$$

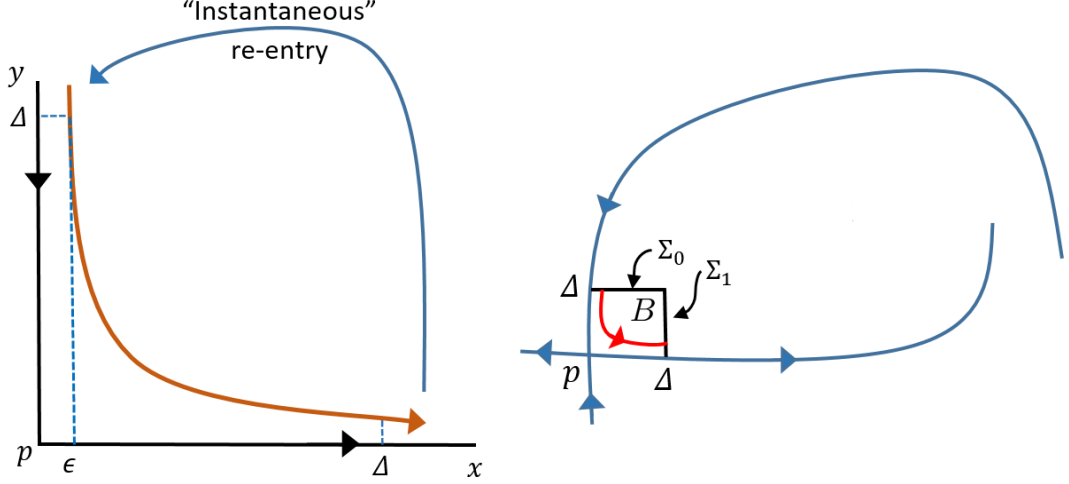


Fig. 3. Trajectory near a homoclinic bifurcation. The left panel shows the trajectory near the saddle point. The right panel shows the Poincaré sections used in the analysis.

Here \hat{x} and \hat{y} represent the unit vectors in the x and y directions, respectively. As $\mu \rightarrow 0$, $\epsilon \rightarrow 0$, thus the first term in the left hand side and the right hand side term in above equation go to zero. Thus we get $Z_{y_0} \approx 0$ near the bifurcation point, and the PRC is only significant in the x -direction. Since the isochrons are orthogonal to the PRC on the limit cycle, the eigenvector $v \approx 0 \hat{x} + 1 \hat{y}$. We will use this information for the normalization condition of the IRC later. Since the trajectory spends most of its time inside the box B , we get $k = \lambda_s + \lambda_u$ by the mean of the divergence of the linear vector field inside B . We will also prove this by the following Poincaré analysis.

Consider the Poincaré maps

$$P = P_2 \circ P_1 : \Sigma_0 \rightarrow \Sigma_0, \quad \text{where} \quad (24)$$

$$P_1 : \Sigma_0 \rightarrow \Sigma_1; \quad (x, \Delta) \rightarrow (\Delta, \Delta e^{\lambda_s T}), \quad (25)$$

$$P_2 : \Sigma_1 \rightarrow \Sigma_0; \quad (\Delta, y) \rightarrow (x, \Delta). \quad (26)$$

The Poincaré sections Σ_0 and Σ_1 are shown in the right panel of Fig. 3. Following the analysis in Chapter 10 of [31], we get the Poincaré map P as

$$P : \Sigma_0 \rightarrow \Sigma_0, \quad (x, \Delta) \rightarrow (Ax^{-\frac{\lambda_s}{\lambda_u}} + \mu, \Delta), \quad (27)$$

where A is a positive constant, and μ is the bifurcation parameter. We note that by Proposition 3.2.8 of [32], the difference between this Poincaré map, obtained by considering the linearized vector field (19,20), and the exact Poincaré map without using this linear approximation is $\mathcal{O}(\Delta^2)$. Moreover, when the periodic orbit is strongly attracting, (27) shows that the fixed point of the Poincaré map, corresponding to the periodic orbit, occurs at $\epsilon \approx \mu$. Equation (27) also gives the nontrivial Floquet multiplier of the periodic orbit as

$$\lambda = A' \epsilon^{-\frac{\lambda_s}{\lambda_u} - 1}, \quad (28)$$

where $A' = -A\lambda_s/\lambda_u$. From this equation, it is easy to see that $\lambda \rightarrow 0$ as $\epsilon \rightarrow 0$. Also note that although the isochrons in the box B may not be horizontal, we have calculated the nontrivial Floquet multiplier for a horizontal section, as that is more convenient; the value of the nontrivial Floquet multiplier is independent of the Poincaré section [31]. k can be found as

$$k = \frac{\log \left(A' \epsilon^{-\frac{\lambda_s}{\lambda_u} - 1} \right)}{T}. \quad (29)$$

Near the bifurcation, this can be written as

$$k = \lim_{\epsilon \rightarrow 0} \frac{\log \left(A' \epsilon^{-\frac{\lambda_s}{\lambda_u} - 1} \right)}{\frac{1}{\lambda_u} \log \left(\frac{\Delta}{\epsilon} \right)}. \quad (30)$$

Since both the numerator and denominator approach plus or minus infinity as $\epsilon \rightarrow 0$, the limit can be solved by L'Hospital's rule as

$$\begin{aligned} k &= \lim_{\epsilon \rightarrow 0} \left(\frac{\lambda_u \Delta \epsilon^{-1}}{A' \epsilon^{-\frac{\lambda_s}{\lambda_u} - 1}} \right) \left(\frac{A' \left(\frac{\lambda_s}{\lambda_u} + 1 \right) \epsilon^{-\frac{\lambda_s}{\lambda_u} - 2}}{\Delta \epsilon^{-2}} \right) \\ &= \lambda_s + \lambda_u. \end{aligned} \quad (31)$$

With this, we get the following adjoint equation for the IRC:

$$\dot{\mathcal{I}}_x = \lambda_s \mathcal{I}_x, \quad (32)$$

$$\dot{\mathcal{I}}_y = \lambda_u \mathcal{I}_y, \quad (33)$$

$$\Rightarrow \mathcal{I}_x = \mathcal{I}_{x_0} e^{\lambda_s t}, \quad (34)$$

$$\mathcal{I}_y = \mathcal{I}_{y_0} e^{\lambda_u t}. \quad (35)$$

The normalization condition $\mathcal{I}_{x_0, y_0} \cdot v = 1$ gives the IRC as

$$\mathcal{I}_{x,y} = \mathcal{I}_{x_0} e^{\frac{\lambda_s \theta}{\omega}} \hat{x} + e^{\frac{\lambda_u \theta}{\omega}} \hat{y}. \quad (36)$$

Here \mathcal{I}_{x_0} remains indeterminate as we do not model the dynamics outside B . The x component of the IRC decreases at an exponential rate, while the y component increases at an exponential rate inside the box B . We do not implement the condition of T -periodicity on (34, 35), as the calculated expressions of the IRC are valid only in the box B . We expect the IRC to jump back to its initial value as the trajectory re-enters the box. As the parameter μ moves away from the bifurcation at $\mu = 0$, corrections to k in (31) come in at $\mathcal{O}(\mu)$ (recall that ϵ is $\mathcal{O}(\mu)$ when the periodic orbit is strongly attracting), so our expression (36) for the IRC will also have $\mathcal{O}(\mu)$ corrections.

3.1.1 A simple model for homoclinic bifurcation

We use a 2-dimensional model derived from [33] to validate our result:

$$\begin{aligned} \dot{x} &= (a + b - 0.5\mu)x - 0.5\mu y - (a/4 + 3b/8)(x + y)^2 - 3a/8(x^2 - y^2), \\ \dot{y} &= 0.5\mu x + (a - b + 0.5\mu)y + (-a/4 + 3b/8)(x + y)^2 + 3a/8(x^2 - y^2). \end{aligned}$$

This system undergoes a homoclinic bifurcation at $\mu = 0$, and has a stable periodic orbit for $\mu > 0$, $a < 0 < b$, and $|b| > |a|$. With parameters $\mu = 1 \times 10^{-13}$, $a = -1$, and $b = 2$, we get a stable periodic orbit with the period $T = 31.7689$, eigenvalues $\lambda_s = -3$, $\lambda_u = 1$, nontrivial Floquet exponent $k = -1.7579$, and the eigenvector $v = 0.0006\hat{x} + 0.9999\hat{y}$. The time series, periodic orbit, and the box B are shown in Fig. 4.

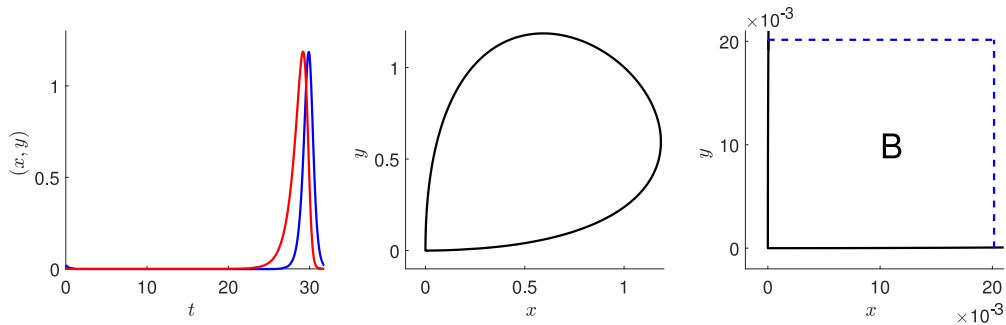


Fig. 4. Periodic orbit near homoclinic bifurcation with parameters $\mu = 1 \times 10^{-13}$, $a = -1$, and $b = 2$. The left (resp., middle) panel shows the time series (resp., orbit). The red and the blue lines show the x and y component of trajectories respectively. The right panel shows the box B .

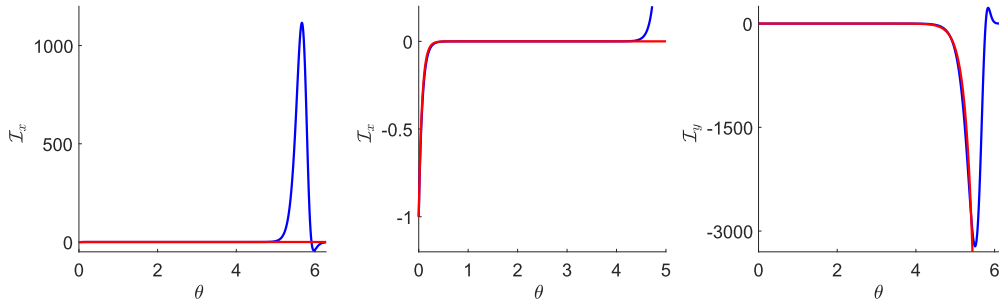


Fig. 5. IRC for periodic orbit near a homoclinic bifurcation. The left and the right panels show the x and y component of the IRC respectively, the middle panel shows the zoomed in plot of the left panel. The blue line shows the numerically computed IRC, while the red line shows an exponential curve with rate constant given by (36).

With $\Delta = 0.0201$, the trajectory spends 86.5 % of its period in the box B . Figure 5 compares the numerically computed IRC with the exponential curve having rate constants from the analytical IRC (36). We see that the numerically computed IRC agrees well with the analytical one in the beginning (inside box B), but diverges after. It oscillates quickly back to its initial value at the end of its period, as is expected.

3.2 Relaxation oscillator

For a relaxation oscillator, at least one variable evolves at a much faster rate than the other variables. Such oscillators are ubiquitous in conductance-based models of cells, where the gating variables evolve at a much slower rate than the cell membrane potential. We will consider the two-dimensional system

$$\mu \dot{x} = f(x, y), \quad 0 < \mu \ll 1, \quad (37)$$

$$\dot{y} = g(x, y). \quad (38)$$

describing a relaxation oscillation as shown in panel (a) of Fig. 6 for small but finite μ , and in panel (b) for the singular limit $\mu = 0$. We assume that the critical manifold for this system, defined implicitly by the equation $f(x, y) = 0$, is an S-shaped curve $y = h(x)$ with exactly two fold points a_1 and a_2 satisfying [21]

$$f(a_i) = 0, \quad f_x(a_i) = 0, \quad f_{xx}(a_i) \neq 0, \quad f_y(a_i) \neq 0, \quad g(a_i) \neq 0, \quad i = 1, 2. \quad (39)$$

We assume that these are the only two points in phase space for which both $f(x, y) = 0$ and $f_x(x, y) = 0$, which is commonly true for relaxation oscillators. It is useful to think of the trajectory for the relaxation oscillation as hugging the left branch of the critical manifold as it moves with $\dot{y} < 0$, then jumping from a_1 to b_1 , then hugging the right branch of the critical manifold as it moves with $\dot{y} > 0$, then jumping from a_2 to b_2 .

In the singular limit ($\mu \rightarrow 0$), the PRC is given as [22]

$$\mathcal{Z}(\theta) = -\frac{\omega g_x}{f_x g} \hat{x} + \frac{\omega}{g} \hat{y} \quad (40)$$

away from the jumps. Here the functions g, g_x , and f_x are evaluated on the periodic orbit, and thus are functions of θ .

At the jumps, which are discontinuities in the trajectory, [22]

$$\mathcal{Z}(\tilde{\theta}_j) = \frac{\omega}{f_y(a_j)} \left(\frac{1}{g(a_j)} - \frac{1}{g(b_j)} \right) \delta(\theta - \tilde{\theta}_j) \hat{x} + \frac{\omega}{g(a_j)} \hat{y}, \quad (41)$$

where $\tilde{\theta}_j$ is the value of the phase corresponding to the point a_j .

The eigenvector v in the direction of the isochron is given as

$$v = \frac{-\hat{x} - \frac{g_x}{f_x} \hat{y}}{\sqrt{1 + \frac{g_x^2}{f_x^2}}}. \quad (42)$$

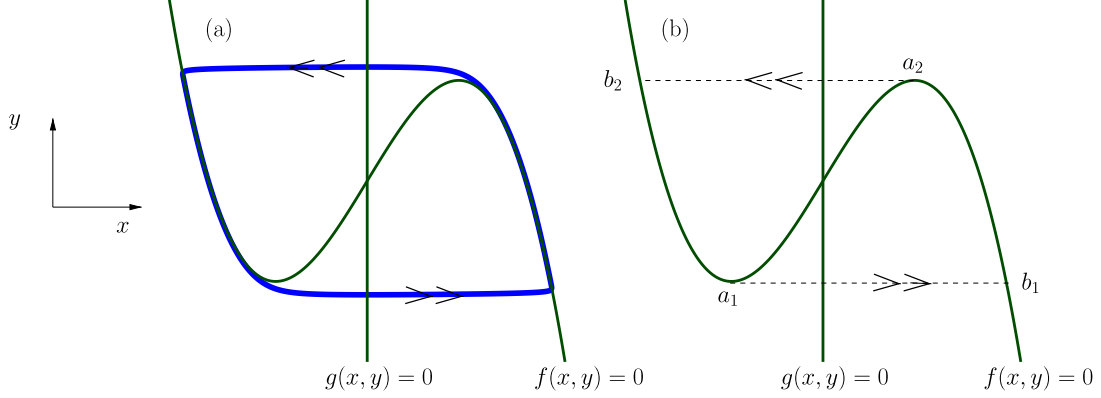


Fig. 6. Relaxation oscillation shown for (a) $0 < \mu \ll 1$ and (b) the singular limit $\mu \rightarrow 0$. The curve implicitly defined by $f(x, y) = 0$ is called the critical manifold, and has folds at the points a_1 and a_2 .

For computing the adjoint equation for IRC in relaxation limit, we do the following analysis in the spirit of [4].

Consider an infinitesimal perturbation $\Delta \mathbf{x} = (\Delta x, \Delta y)$ to the periodic trajectory $\mathbf{x} \in \gamma(t)$. Then the perturbed trajectory evolves as

$$\mu \dot{\Delta x} = f_x \Delta x + f_y \Delta y, \quad (43)$$

$$\dot{\Delta y} = g_x \Delta x + g_y \Delta y. \quad (44)$$

This can be written as $A \dot{\Delta \mathbf{x}} = DF \Delta \mathbf{x}$, where $A = \begin{bmatrix} \mu & 0 \\ 0 & 1 \end{bmatrix}$, and DF is the Jacobian evaluated on the periodic orbit. The isostable shift $\Delta \psi$ by a perturbation $A \Delta \mathbf{x}$ is given by $\Delta \psi = \langle \nabla \psi, A \Delta \mathbf{x} \rangle$, where $\langle \cdot, \cdot \rangle$ is the Euclidean inner product. Its time evolution can be written as

$$\begin{aligned} \dot{\Delta \psi} &= \langle \nabla \dot{\psi}, A \Delta \mathbf{x} \rangle + \langle \nabla \psi, A \dot{\Delta \mathbf{x}} \rangle = k \Delta \psi, \\ &= \langle A^T \nabla \dot{\psi}, \Delta \mathbf{x} \rangle = \langle k A^T \nabla \psi, \Delta \mathbf{x} \rangle - \langle \nabla \psi, DF \Delta \mathbf{x} \rangle, \\ \Rightarrow \quad &\langle A^T \nabla \dot{\psi}, \Delta \mathbf{x} \rangle = \langle k A^T \nabla \psi, \Delta \mathbf{x} \rangle - \langle DF^T \nabla \psi, \Delta \mathbf{x} \rangle. \end{aligned}$$

Since the last equation is valid for an arbitrary perturbation $\Delta \mathbf{x}$, we must have

$$A^T \nabla \dot{\psi} = k A^T \nabla \psi - DF^T \nabla \psi, \quad (45)$$

which can be rewritten as

$$\mu \dot{\mathcal{I}}_x = (k\mu - f_x) \mathcal{I}_x - g_x \mathcal{I}_y, \quad (46)$$

$$\dot{\mathcal{I}}_y = -f_y \mathcal{I}_x + (k - g_y) \mathcal{I}_y, \quad (47)$$

where $\mathcal{I}_x = \partial \psi / \partial x$, and $\mathcal{I}_y = \partial \psi / \partial y$. From the mean of the divergence of the vector field along periodic trajectory, we get the nontrivial Floquet exponent and multiplier as

$$\lambda = \exp \left(\int_0^T (f_x / \mu + g_y) dt \right), \quad (48)$$

$$k = C / \mu + B, \quad (49)$$

where $C = \int_0^T f_x dt$, and $B = \int_0^T g_y dt$. We must have $k < 0$ for a stable periodic orbit. This implies that $C < 0$, because otherwise, k would become positive as $\mu \rightarrow 0$. Thus in the relaxation limit, $k \rightarrow -\infty$ and $\lambda \rightarrow 0$, and any perturbation from the periodic orbit gets nullified instantly by the vector field. The adjoint equation for the IRC becomes

$$\mu \dot{\mathcal{I}}_x = (C + \mu B - f_x) \mathcal{I}_x - g_x \mathcal{I}_y, \quad (50)$$

$$\dot{\mathcal{I}}_y = -f_y \mathcal{I}_x + (C / \mu + B - g_y) \mathcal{I}_y. \quad (51)$$

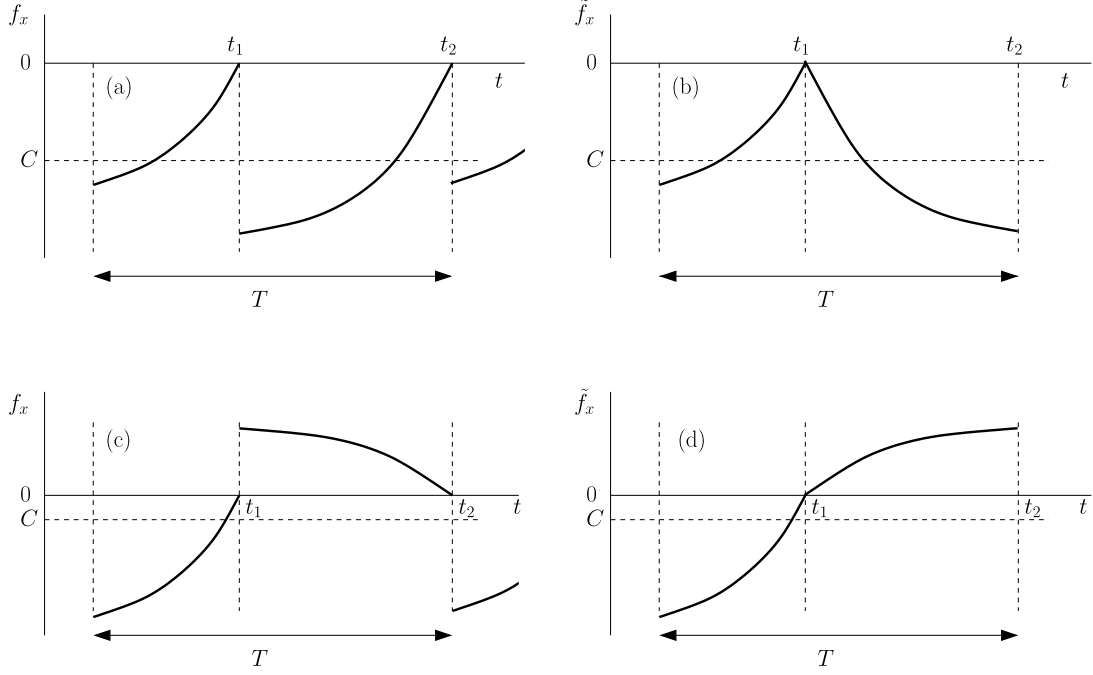


Fig. 7. (a) shows an example time series for f_x evaluated along the relaxation oscillation for one period. The discontinuities correspond to the jumps in the trajectory at times t_1 and t_2 . The function \tilde{f}_x shown in (b) is obtained by reflecting the part of the time series between times t_1 and t_2 about $t = (t_1 + t_2)/2$ to form a continuous function with the same time-average C as f_x . Similar for panels (c) and (d). Since the function \tilde{f}_x is continuous, we can apply the mean value theorem to it.

$$\Rightarrow \mathcal{I}_x = \frac{g_x}{C + \mu B - f_x} \mathcal{I}_y + \mathcal{O}(\mu), \quad (52)$$

$$\Rightarrow \mu \dot{\mathcal{I}}_y = \left(C + \mu B - \mu g_y - \frac{\mu g_x f_y}{C + \mu B - f_x} \right) \mathcal{I}_y + \mathcal{O}(\mu^2). \quad (53)$$

In the singular limit ($\mu \rightarrow 0$), we get

$$(C - f_x) \mathcal{I}_y = 0. \quad (54)$$

Because the trajectory is discontinuous in this limit, the function f_x (which is evaluated on the trajectory) is also discontinuous. However, we note that as the trajectory moves along the critical manifold (on which $f = 0$), f_x is only zero at the fold points. With this in mind, we show two example time series for f_x in Figs. 7(a) and (c), where t_1 and t_2 are the times at which jumps occur during one period of the oscillation. We can obtain a continuous function \tilde{f}_x with the same average value C by reflecting the part of the time series between times t_1 and t_2 as shown in panels (b) and (d) of Fig. 7. The mean value theorem applied to \tilde{f}_x implies that there is at least one phase $\tilde{\theta}_i$ where $C = \tilde{f}_x$, but by construction this also implies that there is at least one phase θ_i where $C = f_x$. Thus, in order to satisfy (54), \mathcal{I}_y has to be zero for all θ except at θ_i , where it can be non-zero. The same can be said about \mathcal{I}_x from (52). Thus we can write the IRC as

$$\mathcal{I}_{x,y} = \left(\sum_i \mathcal{I}_x(\theta_i) \right) \hat{x} + \left(\sum_i \mathcal{I}_y(\theta_i) \right) \hat{y}, \quad (55)$$

where the θ_i are points where $C = f_x$. We note that unlike the PRC, the IRC does not have a delta function at the jumps, because its value is always zero except at the points θ_i , which generically do not correspond to the jumps. It makes sense intuitively that the IRC is zero everywhere except at few points where $C = f_x$ because the periodic orbit is very strongly stable in the relaxation limit (the nontrivial Floquet multiplier is close to zero). Therefore, a perturbation from the periodic orbit gets nullified instantaneously by the stabilizing vector field. This renders the isostable coordinate zero near the periodic orbit, and its gradient zero almost everywhere on the periodic orbit.

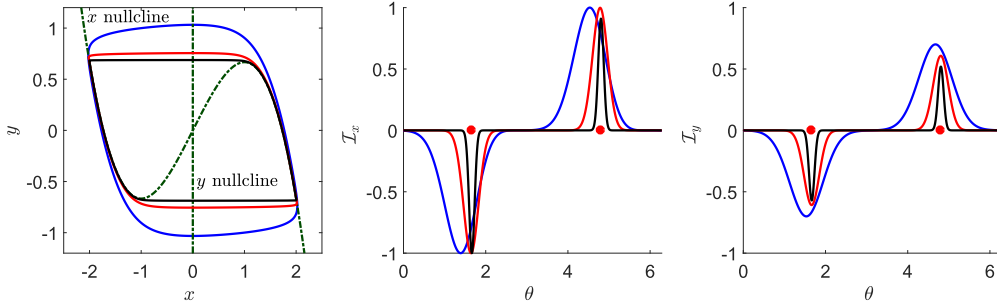


Fig. 8. van der Pol Oscillator: The left panel plots the periodic orbits and nullclines. The middle (resp., the right) panel plots \mathcal{I}_x (resp., \mathcal{I}_y). In all plots, the blue, red and black lines correspond to $\mu = 0.1, 0.01,$ and $0.001,$ respectively. The two red dots in the middle and right panels mark the phases θ_1 and θ_2 .

3.2.1 van der Pol oscillator

An example of a relaxation oscillator is the van der Pol oscillator [34, 35] which can be written as

$$\mu \dot{x} = -y + x - x^3/3, \quad 0 < \mu \ll 1, \quad (56)$$

$$\dot{y} = x. \quad (57)$$

In the relaxation limit ($\mu \rightarrow 0$), we find numerically that $C - f_x$ crosses zero at $\theta_1 = 1.6567$ and $\theta_2 = 4.7983$. Thus we expect the IRC to be zero everywhere except these two θ_i values. We compute periodic orbits and their IRCs for three different values of the parameter μ : 0.1, 0.01, and 0.001, as shown in Fig. 8. We see from Fig. 8 that as μ approaches the relaxation limit, the IRC becomes zero everywhere except near the phases θ_1 , and θ_2 , thus validating our analytical results. Since the IRC is zero everywhere except near 2 points, we do not use the normalization condition of Section 2.2; instead we normalize the IRC by the maximum absolute value of $\{\mathcal{I}_x(\theta_i), \mathcal{I}_y(\theta_i)\}$.

4. Discussion and conclusions

Standard phase reduction is a crucial tool in the analysis and control of oscillators. It reduces the dimensionality of a system, and can make its control experimentally amenable. However it only allows a small perturbation without the risk of driving the oscillator away from the periodic orbit. This limitation makes it unsuitable for some control purposes, especially when a significant control stimulus is required or when a nontrivial Floquet exponent of the periodic orbit has small magnitude. This necessitates the use of the augmented phase reduction.

In this article, we have derived expressions for the augmented phase reduction for two distinct systems with a periodic orbit. We find that for a system near homoclinic bifurcation, the IRC is exponential for a large part of its phase. For a relaxation oscillator, the IRC is zero everywhere except at a few points. We simulated dynamic models which are examples of these two systems, and found that their numerically computed IRCs match with their analytical counterparts very closely.

For a strongly stable system, the nontrivial Floquet exponent k goes to $-\infty$. This is the case for relaxation oscillator in the relaxation limit. Thus, any perturbation to the periodic orbit gets nullified instantly. In such a case, it is not necessary to use the augmented phase reduction, instead the standard phase reduction would suffice. On the other hand, for systems undergoing a homoclinic bifurcation, as was the case for the $\lambda - \omega$, Hopf, and Bautin normal form systems and the example near a SNIPER bifurcation [10], it is better to use the augmented phase reduction over the standard phase reduction, especially when k is a negative number that is small in magnitude.

Acknowledgments

This work was supported by National Science Foundation Grant No. NSF-1264535/1631170.

References

- [1] A.T. Winfree, “Biological rhythms and the behavior of populations of coupled oscillators,” *Journal of Theoretical Biology*, vol. 16, no. 1, pp. 15–42, 1967.
- [2] J. Guckenheimer, “Isochrons and phaseless sets,” *Journal of Mathematical Biology*, vol. 1, no. 3, pp. 259–273, 1975.
- [3] Y. Kuramoto, “Phase-and center-manifold reductions for large populations of coupled oscillators with application to non-locally coupled systems,” *International Journal of Bifurcation and Chaos*, vol. 7, no.04, pp. 789–805, 1997.
- [4] E. Brown, J. Moehlis, and P. Holmes, “On the phase reduction and response dynamics of neural oscillator populations,” *Neural Comp.*, vol. 16, pp. 673–715, 2004.
- [5] J. Moehlis, E. Shea-Brown, and H. Rabitz, “Optimal inputs for phase models of spiking neurons,” *Journal of Computational and Nonlinear Dynamics*, vol. 1, no. 4, pp. 358–367, 2006.
- [6] D. Wilson and J. Moehlis, “Optimal chaotic desynchronization for neural populations,” *SIAM Journal on Applied Dynamical Systems*, vol. 13, no. 1, p. 276, 2014.
- [7] A. Zlotnik, Y. Chen, I.Z. Kiss, H. Tanaka, and Jr-S. Li, “Optimal waveform for fast entrainment of weakly forced nonlinear oscillators,” *Physical Review Letters*, vol. 111, no. 2, 024102, 2013.
- [8] P.A. Tass, *Phase Resetting in Medicine and Biology: Stochastic Modelling and Data Analysis*, Number 7389, Springer Science & Business Media, 2007.
- [9] D.S. Minors, J.M. Waterhouse, and A. Wirz-Justice, “A human phase-response curve to light,” *Neuroscience Letters*, vol. 133, no. 1, pp. 36–40, 1991.
- [10] B. Monga, D. Wilson, T. Matchen, and J. Moehlis, “Phase reduction and phase-based optimal control for biological systems: A tutorial,” *Biological Cybernetics*, vol. 113, no. 1, pp. 11–46, April 2019.
- [11] T. Stigen, P. Danzl, J. Moehlis, and T. Netoff, “Controlling spike timing and synchrony in oscillatory neurons,” *Journal of Neurophysiology*, vol. 105, no. 5, 2074, 2011.
- [12] A. Nabi, T. Stigen, J. Moehlis, and T. Netoff, “Minimum energy control for in vitro neurons,” *Journal of Neural Engineering*, vol. 10, no. 3, 036005, 2013.
- [13] R. Snari, M.R. Tinsley, D. Wilson, S. Faramarzi, T.I. Netoff, J. Moehlis, and K. Showalter, “Desynchronization of stochastically synchronized chemical oscillators,” *Chaos: An Interdisciplinary Journal of Nonlinear Science*, vol. 25, no. 12, 123116, 2015.
- [14] T. Netoff, M.A. Schwemmer, and T.J. Lewis, “Experimentally estimating phase response curves of neurons: theoretical and practical issues,” In *Phase Response Curves in Neuroscience*, pp. 95–129. Springer, 2012.
- [15] J. Guckenheimer and P.J. Holmes, *Nonlinear Oscillations, Dynamical Systems and Bifurcations of Vector Fields*, Springer-Verlag, New York, 1983.
- [16] D. Wilson and J. Moehlis, “Isostable reduction of periodic orbits,” *Physical Review E*, vol. 94, no. 5, 052213, 2016.
- [17] A. Mauroy, I. Mezić, and J. Moehlis, “Isostables, isochrons, and Koopman spectrum for the action–angle representation of stable fixed point dynamics,” *Physica D: Nonlinear Phenomena*, vol. 261, pp. 19–30, 2013.
- [18] S. Shirasaka, W. Kurebayashi, and H. Nakao, “Phase-amplitude reduction of transient dynamics far from attractors for limit-cycling systems,” *Chaos: An Interdisciplinary Journal of Nonlinear Science*, vol. 27, no. 2, 023119, 2017.
- [19] B. Monga and J. Moehlis, “Optimal phase control of biological oscillators using augmented phase reduction,” *Biological Cybernetics*, vol. 113, no. 1, pp. 161–178, April 2019.
- [20] Y.A. Kuznetsov, *Elements of Applied Bifurcation Theory*, Springer-Verlag, New York, third edition, 2013.
- [21] C. Kuehn, *Multiple Time Scale Dynamics*, Springer-Verlag, 2015.
- [22] E.M. Izhikevich, “Phase equations for relaxation oscillators,” *SIAM Journal on Applied Mathematics*, vol. 60, no. 5, pp. 1789–1804, 2000.
- [23] G.B. Ermentrout and N. Kopell, “Multiple pulse interactions and averaging in coupled neural

- oscillators,” *J. Math. Biol.*, vol. 29, pp. 195–217, 1991.
- [24] F.C. Hoppensteadt and E.M. Izhikevich, *Weakly Connected Neural Networks*, Springer-Verlag, New York, 1997.
- [25] B. Ermentrout, *Simulating, Analyzing, and Animating Dynamical Systems: A Guide to XPPAUT for Researchers and Students*, SIAM, Philadelphia, 2002.
- [26] D. Wilson, “Isostable reduction of oscillators with piecewise smooth dynamics and complex Floquet multipliers,” *Phys. Rev. E*, vol. 99, 022210, 2019.
- [27] P. Glendinning, *Stability, Instability and Chaos: An Introduction to the Theory of Nonlinear Differential Equations*, Cambridge Texts in Applied Mathematics, Cambridge University Press, 1994.
- [28] D. Wilson and B. Ermentrout, “Greater accuracy and broadened applicability of phase reduction using isostable coordinates,” *J. Math. Biol.*, vol. 76, pp. 37–66, 2018.
- [29] A. Mauroy and I. Mezić, “Global computation of phase-amplitude reduction for limit-cycle dynamics,” *Chaos: An Interdisciplinary Journal of Nonlinear Science*, vol. 28, no. 7, 073108, 2018.
- [30] K.M. Shaw, Y.-M. Park, H.J. Chiel, and P.J. Thomas, “Phase resetting in an asymptotically phaseless system: On the phase response of limit cycles verging on a heteroclinic orbit,” *SIAM Journal on Applied Dynamical Systems*, vol. 11, no. 1, pp. 250–391, 2012.
- [31] S. Wiggins, *Introduction to Applied Nonlinear Dynamical Systems and Chaos*, Springer-Verlag, New York, 2003.
- [32] S. Wiggins, *Global Bifurcations and Chaos*, Springer-Verlag, 1988.
- [33] B. Sandstede, “Constructing dynamical systems having homoclinic bifurcation points of codimension two,” *Journal of Dynamics and Differential Equations*, vol. 9, no. 2, pp. 269–288, 1997.
- [34] B. Van der Pol, “A theory of the amplitude of free and forced triode vibrations,” *Radio Review*, vol. 1, pp. 701–710, 1920.
- [35] T. Kanamaru, “Van der Pol oscillator,” *Scholarpedia*, vol. 2, no. 1, 2202, 2007. revision #138698.